Chapter 6
Approach with Rectangular Arrays

All what we have done so far with linear arrays is, obviously, not limited to this type of arrays. In this chapter, we show how to extend some of these results to two-dimensional arrays such as the rectangular ones. The focus is on fixed beamforming. Of course, very interesting adaptive beamformers can be derived as well by following the same steps as in previous chapters.

6.1 Signal Model and Problem Formulation

The two-dimensional (2-D) array evaluated in this chapter is a rectangular array (RA) depicted in Fig. 6.1. Considering the Cartesian coordinate system with microphone $(1, 1)$ as its origin, the studied RA is composed of M_x omnidirectional sensors along the x (negative) axis with a uniform interelement spacing equal to δ_x and M_y omnidirectional sensors along the y (negative) axis with a uniform interelement spacing equal to δ_y. Thus, the total number of microphones is equal to $M_x M_y$, whose positions are denoted (m_x, m_y) with $m_x = 1, 2, \ldots, M_x,\ m_y = 1, 2, \ldots, M_y$. Notice that in the direction of the x axis, we have M_y parallel ULAs composed of M_x microphones each with a spacing δ_x, while in the direction of the y axis, we have M_x parallel ULAs composed of M_y microphones each with a spacing δ_y.

We assume that a farfield desired source signal (plane wave) propagates from the azimuth angle, θ, in an anechoic acoustic environment at the speed of sound, i.e., $c = 340$ m/s, and impinges on the above described 2-D array. Then, it is not hard to see that the corresponding steering matrix (of size $M_x \times M_y$) is [1]

J. Benesty et al., *Array Processing*, Springer Topics in Signal Processing 18, https://doi.org/10.1007/978-3-030-15600-8_6

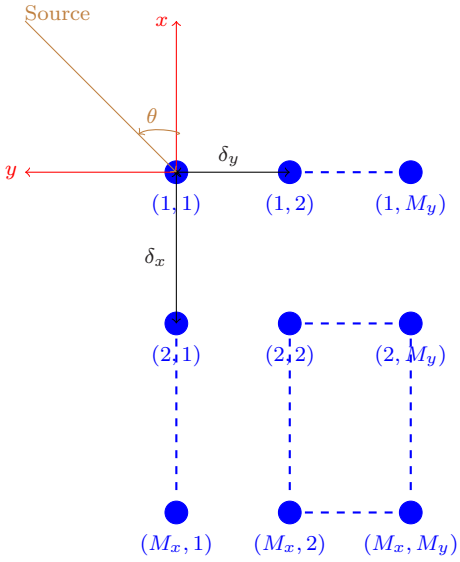

Fig. 6.1 Illustration of the studied 2-D microphone array.

$$\begin{aligned}\mathbf{D}_\theta &= \left[\, D_{y,\theta,1}\mathbf{d}_{x,\theta}\; D_{y,\theta,2}\mathbf{d}_{x,\theta}\; \cdots\; D_{y,\theta,M_y}\mathbf{d}_{x,\theta} \,\right] \\ &= \begin{bmatrix} D_{x,\theta,1}\mathbf{d}_{y,\theta}^T \\ D_{x,\theta,2}\mathbf{d}_{y,\theta}^T \\ \vdots \\ D_{x,\theta,M_x}\mathbf{d}_{y,\theta}^T \end{bmatrix} \\ &= \mathbf{d}_{x,\theta}\mathbf{d}_{y,\theta}^T,\end{aligned} \tag{6.1}$$

where

$$\begin{aligned}\mathbf{d}_{x,\theta} &= \left[\, D_{x,\theta,1}\; D_{x,\theta,2}\; \cdots\; D_{x,\theta,M_x} \,\right]^T \\ &= \left[\, 1\; e^{-\jmath\frac{\omega\delta_x}{c}\cos\theta}\; \cdots\; e^{-\jmath\frac{(M_x-1)\omega\delta_x}{c}\cos\theta} \,\right]^T\end{aligned} \tag{6.2}$$

is the steering vector associated with the x axis,

$$\begin{aligned}\mathbf{d}_{y,\theta} &= \left[\, D_{y,\theta,1}\; D_{y,\theta,2}\; \cdots\; D_{y,\theta,M_y} \,\right]^T \\ &= \left[\, 1\; e^{-\jmath\frac{\omega\delta_y}{c}\sin\theta}\; \cdots\; e^{-\jmath\frac{(M_y-1)\omega\delta_y}{c}\sin\theta} \,\right]^T\end{aligned} \tag{6.3}$$

is the steering vector associated with the y axis.

Thanks to the above steering matrix, the observation signal matrix of size $M_x \times M_y$ of the RA can be expressed in the frequency domain as

$$\begin{aligned}\mathbf{Y} &= \mathbf{X} + \mathbf{V} \\ &= \mathbf{D}_\theta X + \mathbf{V},\end{aligned} \tag{6.4}$$

where X is the zero-mean desired source signal and $\mathbf{V}$ is the zero-mean additive noise signal matrix. Without loss of generality, it is assumed in the rest that the desired source signal propagates from the angle $\theta = 0$ (endfire direction). Therefore, (6.4) becomes

$$\mathbf{Y} = \mathbf{D}_0 X + \mathbf{V}, \tag{6.5}$$

where $\mathbf{D}_0$ is the steering matrix at $\theta = 0$.

Using the convenient vectorization operation, which consists of converting a matrix into a vector, (6.5) can be expressed, equivalently, as

$$\begin{aligned}\text{vec}\,(\mathbf{Y}) &= \left[\mathbf{y}_{:1}^T\ \mathbf{y}_{:2}^T \cdots\ \mathbf{y}_{:M_y}^T\right]^T \\ &= \text{vec}\left(\mathbf{d}_{x,0}\mathbf{d}_{y,0}^T\right) X + \text{vec}\,(\mathbf{V}) \\ &= \mathbf{d}_{y,0} \otimes \mathbf{d}_{x,0} X + \text{vec}\,(\mathbf{V}),\end{aligned} \tag{6.6}$$

where $\mathbf{y}_{:m_y}$ is the m_yth column of $\mathbf{Y}$ and $\text{vec}\,(\mathbf{V})$ is defined similarly to $\text{vec}\,(\mathbf{Y})$. To further simplify the notation, we write $\widetilde{\mathbf{y}} = \text{vec}\,(\mathbf{Y})$, $\widetilde{\mathbf{d}}_\theta = \text{vec}\,(\mathbf{D}_\theta) = \mathbf{d}_{y,\theta} \otimes \mathbf{d}_{x,\theta}$, and $\widetilde{\mathbf{v}} = \text{vec}\,(\mathbf{V})$. With this notation, (6.6) is

$$\widetilde{\mathbf{y}} = \widetilde{\mathbf{d}}_0 X + \widetilde{\mathbf{v}}. \tag{6.7}$$

We deduce that the $M_x M_y \times M_x M_y$ covariance matrix of $\widetilde{\mathbf{y}}$ is

$$\begin{aligned}\mathbf{\Phi}_{\widetilde{\mathbf{y}}} &= E\left(\widetilde{\mathbf{y}}\widetilde{\mathbf{y}}^H\right) \\ &= \widetilde{\mathbf{d}}_0 \widetilde{\mathbf{d}}_0^H \phi_X + \mathbf{\Phi}_{\widetilde{\mathbf{v}}},\end{aligned} \tag{6.8}$$

where $\phi_X = E\left(|X|^2\right)$ is the variance of X and $\mathbf{\Phi}_{\widetilde{\mathbf{v}}} = E\left(\widetilde{\mathbf{v}}\widetilde{\mathbf{v}}^H\right)$ is the covariance matrix of $\widetilde{\mathbf{v}}$.

6.2 2-D Beamforming

The conventional way to perform 2-D beamforming is to apply a complex-valued linear filter, $\mathbf{h}$, of length $M_x M_y$ to the observation signal vector, $\widetilde{\mathbf{y}}$. We get [2]

$$\begin{aligned}Z_{\text{C}} &= \mathbf{h}^H \widetilde{\mathbf{y}} \\ &= \mathbf{h}^H \widetilde{\mathbf{d}}_0 X + \mathbf{h}^H \widetilde{\mathbf{v}},\end{aligned} \tag{6.9}$$

where Z_{C} is the estimate of the desired signal, X. However, there are two main problems with this approach. The first one is the large number of coefficients (equal to $M_x M_y$) that need to be estimated, so complexity can be an issue. More importantly, the second problem has to do with the inversion of very ill-conditioned large matrices in most derived optimal beamformers, which will necessarily lead to serious estimation problems in the presence of uncertainties.

Due to some potential problems with the conventional approach, we propose in this investigation to use two complex-valued linear filters $\mathbf{h}_x$ and $\mathbf{h}_y$ of respective lengths M_x and M_y as follows[1]:

$$\begin{aligned} Z &= \mathbf{h}_x^H \mathbf{Y} \mathbf{h}_y^* \\ &= \left(\mathbf{h}_x^H \mathbf{d}_{x,0}\right) \left(\mathbf{d}_{y,0}^T \mathbf{h}_y^*\right) X + \mathbf{h}_x^H \mathbf{V} \mathbf{h}_y^* \\ &= \left(\mathbf{h}_x^H \mathbf{d}_{x,0}\right) \left(\mathbf{h}_y^H \mathbf{d}_{y,0}\right) X + \mathbf{h}_x^H \mathbf{V} \mathbf{h}_y^*, \end{aligned} \tag{6.10}$$

where Z is the estimate of X. We observe that Z is bilinear in $\mathbf{h}_x^*$ and $\mathbf{h}_y^*$ since, for every fixed $\mathbf{h}_x^*$, it is a linear function of $\mathbf{h}_y^*$ and for every fixed $\mathbf{h}_y^*$, it is a linear function of $\mathbf{h}_x^*$. This bilinear form takes advantage of the structure of the 2-D array and the corresponding steering vectors. We can also express (6.10) as

$$\begin{aligned} Z &= \mathrm{tr}\left(\mathbf{h}_y^* \mathbf{h}_x^H \mathbf{Y}\right) \\ &= \mathrm{tr}\left[\left(\mathbf{h}_x \mathbf{h}_y^T\right)^H \mathbf{Y}\right] \\ &= \mathrm{vec}^H\left(\mathbf{h}_x \mathbf{h}_y^T\right) \mathrm{vec}\left(\mathbf{Y}\right) \\ &= \left(\mathbf{h}_y \otimes \mathbf{h}_x\right)^H \widetilde{\mathbf{y}}, \end{aligned} \tag{6.11}$$

where $\mathrm{tr}(\cdot)$ denotes the trace of a square matrix and $\mathbf{h}_y \otimes \mathbf{h}_x$ is the global beamformer, which is simply the Kronecker product between the two individual beamformers $\mathbf{h}_y$ and $\mathbf{h}_x$ along the y and x axes, respectively. As a consequence, by taking $\mathbf{h} = \mathbf{h}_y \otimes \mathbf{h}_x$ in (6.9), we observe that Kronecker product beamforming is an interesting particular case of the conventional approach, where $\mathbf{h}$ is assumed to have a particular structure. From (6.11), we find that the variance of Z is

$$\begin{aligned} \phi_Z &= \left(\mathbf{h}_y \otimes \mathbf{h}_x\right)^H \mathbf{\Phi}_{\widetilde{\mathbf{y}}} \left(\mathbf{h}_y \otimes \mathbf{h}_x\right) \\ &= \left|\left(\mathbf{h}_y \otimes \mathbf{h}_x\right)^H \widetilde{\mathbf{d}}_0\right|^2 \phi_X + \left(\mathbf{h}_y \otimes \mathbf{h}_x\right)^H \mathbf{\Phi}_{\widetilde{\mathbf{v}}} \left(\mathbf{h}_y \otimes \mathbf{h}_x\right) \\ &= \left|\mathbf{h}_x^H \mathbf{d}_{x,0}\right|^2 \left|\mathbf{h}_y^H \mathbf{d}_{y,0}\right|^2 \phi_X + \left(\mathbf{h}_y \otimes \mathbf{h}_x\right)^H \mathbf{\Phi}_{\widetilde{\mathbf{v}}} \left(\mathbf{h}_y \otimes \mathbf{h}_x\right). \end{aligned} \tag{6.12}$$

[1] Now, the number of coefficients to be estimated is equal to $M_x + M_y$ instead of $M_x M_y$ for the conventional method. If $M_x = M_y = M$, we only need to handle a linear number ($2M$) of coefficients instead of a square number (M^2) of coefficients. So when M is large, the length of the filter in the conventional approach becomes quickly prohibitive.

In the rest, the distortionless constraint is desired, i.e.,

$$\left(\mathbf{h}_x^H \mathbf{d}_{x,0}\right)\left(\mathbf{h}_y^H \mathbf{d}_{y,0}\right) = 1. \tag{6.13}$$

This also means that the value of the Kronecker product beamformer pattern should be equal to 1 at $\theta = 0$ and smaller than 1 at $\theta \neq 0$. In particular, when $\mathbf{h}_x^H \mathbf{d}_{x,0} = \mathbf{h}_y^H \mathbf{d}_{y,0} = 1$, then (6.13) is also verified; so we will always consider this case.

6.3 Performance Measures

The first important measure discussed in this section is the beampattern, which describes the sensitivity of the Kronecker product beamformer to a plane wave impinging on the 2-D array from the direction θ. Mathematically, it is defined as

$$\begin{aligned}\mathcal{B}_\theta\left(\mathbf{h}_y \otimes \mathbf{h}_x\right) &= \left(\mathbf{h}_y \otimes \mathbf{h}_x\right)^H \widetilde{\mathbf{d}}_\theta \\ &= \left(\mathbf{h}_y \otimes \mathbf{h}_x\right)^H \left(\mathbf{d}_{y,\theta} \otimes \mathbf{d}_{x,\theta}\right) \\ &= \left(\mathbf{h}_x^H \mathbf{d}_{x,\theta}\right)\left(\mathbf{h}_y^H \mathbf{d}_{y,\theta}\right) \\ &= \mathcal{B}_{x,\theta}\left(\mathbf{h}_x\right) \times \mathcal{B}_{y,\theta}\left(\mathbf{h}_y\right).\end{aligned} \tag{6.14}$$

It is interesting to observe that the beampattern of the global beamformer is equal to the product of the beampatterns of the individual beamformers. As a result, the nulls of $\mathcal{B}_\theta\left(\mathbf{h}_y \otimes \mathbf{h}_x\right)$ correspond exactly to the nulls of $\mathcal{B}_{x,\theta}\left(\mathbf{h}_x\right)$ and $\mathcal{B}_{y,\theta}\left(\mathbf{h}_y\right)$. In particular, if $\mathcal{B}_{x,\theta}\left(\mathbf{h}_x\right)$ has a null at θ_0 of multiplicity 1 and $\mathcal{B}_{y,\theta}\left(\mathbf{h}_y\right)$ has also a null at θ_0 of multiplicity 1, then $\mathcal{B}_\theta\left(\mathbf{h}_y \otimes \mathbf{h}_x\right)$ has a null in the same direction but of multiplicity 2.

Considering the origin of the Cartesian coordinates as the reference, we define the input SNR with respect to this reference as

$$\text{iSNR} = \frac{\phi_X}{\phi_{V_{11}}}, \tag{6.15}$$

where $\phi_{V_{11}}$ is the variance at the noise reference.

The output SNR is defined as

$$\begin{aligned}\text{oSNR}\left(\mathbf{h}_y \otimes \mathbf{h}_x\right) &= \phi_X \frac{\left|\mathbf{h}_x^H \mathbf{d}_{x,0}\right|^2 \left|\mathbf{h}_y^H \mathbf{d}_{y,0}\right|^2}{\left(\mathbf{h}_y \otimes \mathbf{h}_x\right)^H \mathbf{\Phi}_{\widetilde{\mathbf{v}}} \left(\mathbf{h}_y \otimes \mathbf{h}_x\right)} \\ &= \frac{\phi_X}{\phi_{V_{11}}} \times \frac{\left|\mathbf{h}_x^H \mathbf{d}_{x,0}\right|^2 \left|\mathbf{h}_y^H \mathbf{d}_{y,0}\right|^2}{\left(\mathbf{h}_y \otimes \mathbf{h}_x\right)^H \mathbf{\Gamma}_{\widetilde{\mathbf{v}}} \left(\mathbf{h}_y \otimes \mathbf{h}_x\right)},\end{aligned} \tag{6.16}$$

where

$$\mathbf{\Gamma}_{\widetilde{\mathbf{v}}} = \frac{\mathbf{\Phi}_{\widetilde{\mathbf{v}}}}{\phi_{V_{11}}} \tag{6.17}$$

is the pseudo-coherence matrix of $\widetilde{\mathbf{v}}$.

The definition of the SNR gain is easily derived from the two previous definitions of the input and output SNRs, i.e.,

$$\begin{aligned}\mathcal{G}\left(\mathbf{h}_y \otimes \mathbf{h}_x\right) &= \frac{\text{oSNR}\left(\mathbf{h}_y \otimes \mathbf{h}_x\right)}{\text{iSNR}} \\ &= \frac{\left|\mathbf{h}_x^H \mathbf{d}_{x,0}\right|^2 \left|\mathbf{h}_y^H \mathbf{d}_{y,0}\right|^2}{\left(\mathbf{h}_y \otimes \mathbf{h}_x\right)^H \mathbf{\Gamma}_{\widetilde{\mathbf{v}}} \left(\mathbf{h}_y \otimes \mathbf{h}_x\right)}.\end{aligned} \tag{6.18}$$

The best known way to evaluate the sensitivity of an array to some of its imperfections and other uncertainties is via the WNG, which is defined by taking $\mathbf{\Gamma}_{\widetilde{\mathbf{v}}} = \mathbf{I}_{M_x M_y}$ in (6.18), where $\mathbf{I}_{M_x M_y}$ is the $M_x M_y \times M_x M_y$ identity matrix, i.e.,

$$\begin{aligned}\mathcal{W}\left(\mathbf{h}_y \otimes \mathbf{h}_x\right) &= \frac{\left|\mathbf{h}_x^H \mathbf{d}_{x,0}\right|^2 \left|\mathbf{h}_y^H \mathbf{d}_{y,0}\right|^2}{\left(\mathbf{h}_y \otimes \mathbf{h}_x\right)^H \left(\mathbf{h}_y \otimes \mathbf{h}_x\right)} \\ &= \frac{\left|\mathbf{h}_x^H \mathbf{d}_{x,0}\right|^2}{\mathbf{h}_x^H \mathbf{h}_x} \times \frac{\left|\mathbf{h}_y^H \mathbf{d}_{y,0}\right|^2}{\mathbf{h}_y^H \mathbf{h}_y} \\ &= \mathcal{W}_x\left(\mathbf{h}_x\right) \times \mathcal{W}_y\left(\mathbf{h}_y\right).\end{aligned} \tag{6.19}$$

Since $\mathcal{W}_x\left(\mathbf{h}_x\right) \leq M_x$ and $\mathcal{W}_y\left(\mathbf{h}_y\right) \leq M_y$, we deduce that $\mathcal{W}\left(\mathbf{h}_y \otimes \mathbf{h}_x\right) \leq M_x M_y$.

Another important measure, which quantifies how the 2-D microphone array performs in the presence of reverberation is the DF. For the spherically isotropic noise field, the definition of the DF is

$$\mathcal{D}\left(\mathbf{h}_y \otimes \mathbf{h}_x\right) = \frac{\left|\mathbf{h}_x^H \mathbf{d}_{x,0}\right|^2 \left|\mathbf{h}_y^H \mathbf{d}_{y,0}\right|^2}{\left(\mathbf{h}_y \otimes \mathbf{h}_x\right)^H \widetilde{\mathbf{\Gamma}} \left(\mathbf{h}_y \otimes \mathbf{h}_x\right)}, \tag{6.20}$$

where

$$\widetilde{\mathbf{\Gamma}} = \begin{bmatrix} \mathbf{\Gamma}_1 & \mathbf{\Gamma}_2 & \cdots & \mathbf{\Gamma}_{M_y-1} & \mathbf{\Gamma}_{M_y} \\ \mathbf{\Gamma}_2 & \mathbf{\Gamma}_1 & \cdots & \mathbf{\Gamma}_{M_y-2} & \mathbf{\Gamma}_{M_y-1} \\ \vdots & \vdots & \ddots & \vdots & \vdots \\ \mathbf{\Gamma}_{M_y-1} & \mathbf{\Gamma}_{M_y-2} & \cdots & \mathbf{\Gamma}_1 & \mathbf{\Gamma}_2 \\ \mathbf{\Gamma}_{M_y} & \mathbf{\Gamma}_{M_y-1} & \cdots & \mathbf{\Gamma}_2 & \mathbf{\Gamma}_1 \end{bmatrix} \tag{6.21}$$

is a symmetric block Toeplitz matrix and the elements of the M_y symmetric Toeplitz matrices $\mathbf{\Gamma}_{m_y},\ m_y = 1, 2, \ldots, M_y$ (of size $M_x \times M_x$) are given by

$$\left(\mathbf{\Gamma}_{m_y}\right)_{ij} = \operatorname{sinc}\left[\frac{\omega\sqrt{(i-j)^2\delta_x^2 + \left(m_y-1\right)^2\delta_y^2}}{c}\right], \tag{6.22}$$

with $i, j = 1, 2, \ldots, M_x$ and $\operatorname{sinc} x = \sin x/x$. It is clear that $\mathcal{D}\left(\mathbf{h}_y \otimes \mathbf{h}_x\right) \leq \widetilde{\mathbf{d}}_0^H \widetilde{\mathbf{\Gamma}}^{-1} \widetilde{\mathbf{d}}_0$. Using the fact that

$$\begin{aligned} \mathbf{h}_y \otimes \mathbf{h}_x &= \left(\mathbf{h}_y \otimes \mathbf{I}_{M_x}\right)\mathbf{h}_x \\ &= \left(\mathbf{I}_{M_y} \otimes \mathbf{h}_x\right)\mathbf{h}_y, \end{aligned} \tag{6.23}$$

where $\mathbf{I}_{M_x}$ and $\mathbf{I}_{M_y}$ are the identity matrices of sizes $M_x \times M_x$ and $M_y \times M_y$, respectively, we can rewrite the DF as

$$\mathcal{D}\left(\mathbf{h}_y \otimes \mathbf{h}_x\right) = \frac{\left|\mathbf{h}_x^H \mathbf{d}_{x,0}\right|^2 \left|\mathbf{h}_y^H \mathbf{d}_{y,0}\right|^2}{\mathbf{h}_x^H \mathbf{\Gamma}_y \mathbf{h}_x} \tag{6.24}$$

and

$$\mathcal{D}\left(\mathbf{h}_y \otimes \mathbf{h}_x\right) = \frac{\left|\mathbf{h}_x^H \mathbf{d}_{x,0}\right|^2 \left|\mathbf{h}_y^H \mathbf{d}_{y,0}\right|^2}{\mathbf{h}_y^H \mathbf{\Gamma}_x \mathbf{h}_y}, \tag{6.25}$$

where

$$\mathbf{\Gamma}_y = \left(\mathbf{h}_y \otimes \mathbf{I}_{M_x}\right)^H \widetilde{\mathbf{\Gamma}} \left(\mathbf{h}_y \otimes \mathbf{I}_{M_x}\right) \tag{6.26}$$

and

$$\mathbf{\Gamma}_x = \left(\mathbf{I}_{M_y} \otimes \mathbf{h}_x\right)^H \widetilde{\mathbf{\Gamma}} \left(\mathbf{I}_{M_y} \otimes \mathbf{h}_x\right). \tag{6.27}$$

If the filter $\mathbf{h}_y$ is fixed and distortionless, i.e., $\mathbf{h}_y^H \mathbf{d}_{y,0} = 1$, we write (6.24) as

$$\mathcal{D}\left(\mathbf{h}_x | \mathbf{h}_y\right) = \frac{\left|\mathbf{h}_x^H \mathbf{d}_{x,0}\right|^2}{\mathbf{h}_x^H \mathbf{\Gamma}_y \mathbf{h}_x}, \tag{6.28}$$

and if the filter $\mathbf{h}_x$ is fixed and distortionless, i.e., $\mathbf{h}_x^H \mathbf{d}_{x,0} = 1$, we write (6.25) as

$$\mathcal{D}\left(\mathbf{h}_y | \mathbf{h}_x\right) = \frac{\left|\mathbf{h}_y^H \mathbf{d}_{y,0}\right|^2}{\mathbf{h}_y^H \mathbf{\Gamma}_x \mathbf{h}_y}. \tag{6.29}$$

6.4 Fixed Beamformers

There is a myriad of fixed Kronecker product beamformers that we can derive from the proposed approach. Here, we give some relevant examples, which are mostly deduced from the above performance measures.

6.4.1 Delay and Sum

The definition of the WNG with the conventional approach is

$$\mathcal{W}(\mathbf{h}) = \frac{\left|\mathbf{h}^H \widetilde{\mathbf{d}}_0\right|^2}{\mathbf{h}^H \mathbf{h}}, \tag{6.30}$$

whose maximization gives the very well-known DS beamformer:

$$\begin{aligned} \mathbf{h}_{\mathrm{DS}} &= \frac{\widetilde{\mathbf{d}}_0}{\widetilde{\mathbf{d}}_0^H \widetilde{\mathbf{d}}_0} \\ &= \frac{\mathbf{d}_{y,0} \otimes \mathbf{d}_{x,0}}{M_x M_y} \end{aligned} \tag{6.31}$$

and the corresponding WNG is, obviously,

$$\mathcal{W}(\mathbf{h}_{\mathrm{DS}}) = M_x M_y. \tag{6.32}$$

Now, from the maximization of the WNG in (6.19) with respect to $\mathbf{h}_x$ and $\mathbf{h}_y$, we obtain

$$\mathbf{h}_{x,\mathrm{DS}} = \frac{\mathbf{d}_{x,0}}{M_x}, \tag{6.33}$$

$$\mathbf{h}_{y,\mathrm{DS}} = \frac{\mathbf{d}_{y,0}}{M_y}. \tag{6.34}$$

As a result, the global beamformer is

$$\mathbf{h}_{y,\mathrm{DS}} \otimes \mathbf{h}_{x,\mathrm{DS}} = \mathbf{h}_{\mathrm{DS}}, \tag{6.35}$$

showing that the DS beamformers with the conventional and Kronecker product approaches coincide and the number of nulls in the corresponding beampattern is smaller than $M_x + M_y - 2$. For $M_x = M_y = M$, $\mathcal{W}(\mathbf{h}_{y,\mathrm{DS}} \otimes \mathbf{h}_{x,\mathrm{DS}}) = M^2$ with only $2M$ coefficients. This shows how the redundancy in an RA is taken advantage of.

Figure 6.2 displays the directivity patterns of the DS beamformer, $\mathbf{h}_{\mathrm{DS}}$, for $f = 2$ kHz, $\delta_x = \delta_y = 2$ cm and different numbers of sensors $M_x = M_y$.

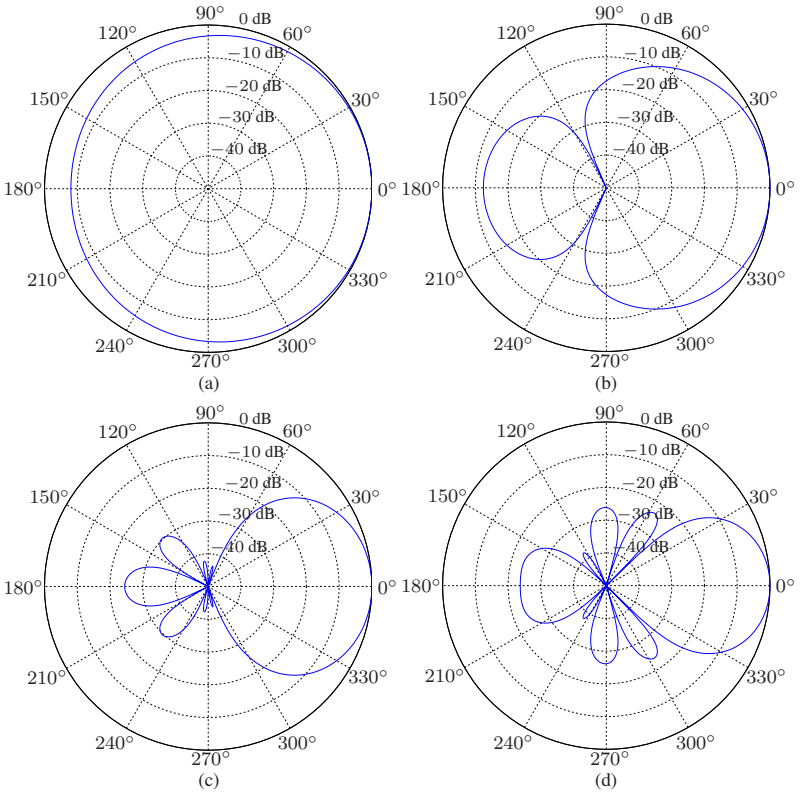

Fig. 6.2 Beampatterns of the DS beamformer, $\mathbf{h}_{\mathrm{DS}}$, for $f = 2$ kHz, $\delta_x = \delta_y = 2$ cm, and different numbers of sensors $M_x = M_y$: (a) $M_x = M_y = 3$, (b) $M_x = M_y = 6$, (c) $M_x = M_y = 9$, and (d) $M_x = M_y = 12$.

Figure 6.3 shows plots of the DFs and WNGs of the DS beamformer as a function of frequency for $\delta_x = \delta_y = 2$ cm and different numbers of sensors $M_x = M_y$. We observe that as the number of sensors increases, the width of the main beam decreases, and both the DF and the WNG of the DS beamformer increase.

6.4.2 Combined Superdirective/Delay and Sum

In this subsection, we show how to combine the superdirective and DS beamformers in a 2-D array in order to take advantage of the best of them. Indeed, for a ULA with the desired source at the endfire, it is well known that the superdirective maximizes the DF but amplifies the white noise while the DS maximizes the WNG but gives poor levels of the DF [3], [4], [5]. Therefore,

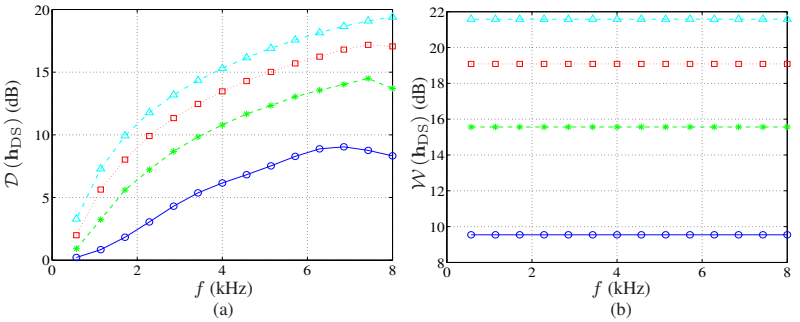

Fig. 6.3 Performance of the DS beamformer, $\mathbf{h}_{\mathrm{DS}}$, as a function of frequency for $\delta_x = \delta_y = 2$ cm and different numbers of sensors $M_x = M_y$: $M_x = M_y = 3$ (solid line with circles), $M_x = M_y = 6$ (dashed line with asterisks), $M_x = M_y = 9$ (dotted line with squares), and $M_x = M_y = 12$ (dash-dot line with triangles). (a) DF and (b) WNG.

in the x axis direction, we propose to use the superdirective beamformer [3], [4]:

$$\mathbf{h}_{x,\mathrm{SD}} = \frac{\boldsymbol{\Gamma}_1^{-1}\mathbf{d}_{x,0}}{\mathbf{d}_{x,0}^H\boldsymbol{\Gamma}_1^{-1}\mathbf{d}_{x,0}}, \tag{6.36}$$

where $\boldsymbol{\Gamma}_1$ is the first block matrix of $\widetilde{\boldsymbol{\Gamma}}$, while in the y axis direction, we take the DS beamformer given in (6.34), i.e., $\mathbf{h}_{y,\mathrm{DS}}$; so that the global beamformer is $\mathbf{h}_{y,\mathrm{DS}} \otimes \mathbf{h}_{x,\mathrm{SD}}$. We deduce that the WNG is

$$\mathcal{W}\left(\mathbf{h}_{y,\mathrm{DS}} \otimes \mathbf{h}_{x,\mathrm{SD}}\right) = M_y \mathcal{W}_x\left(\mathbf{h}_{x,\mathrm{SD}}\right), \tag{6.37}$$

showing that the WNG of the global filter with an RA is improved by a factor of M_y compared to the WNG of the superdirective beamformer with a ULA. The power beampattern is

$$\begin{aligned}\left|\mathcal{B}_\theta\left(\mathbf{h}_{y,\mathrm{DS}} \otimes \mathbf{h}_{x,\mathrm{SD}}\right)\right|^2 &= \left|\mathcal{B}_{x,\theta}\left(\mathbf{h}_{x,\mathrm{SD}}\right)\right|^2 \left|\mathcal{B}_{y,\theta}\left(\mathbf{h}_{y,\mathrm{DS}}\right)\right|^2 \\ &\leq \left|\mathcal{B}_{x,\theta}\left(\mathbf{h}_{x,\mathrm{SD}}, \theta\right)\right|^2,\end{aligned} \tag{6.38}$$

implying that the global beamformer is more directive than the superdirective beamformer. As a consequence,

$$\mathcal{D}\left(\mathbf{h}_{y,\mathrm{DS}} \otimes \mathbf{h}_{x,\mathrm{SD}}\right) \geq \mathcal{D}\left(\mathbf{h}_{x,\mathrm{SD}}\right). \tag{6.39}$$

Figure 6.4 displays the directivity patterns of the combined superdirective/DS beamformer, $\mathbf{h}_{y,\mathrm{DS}} \otimes \mathbf{h}_{x,\mathrm{SD}}$, for $f = 2$ kHz, $\delta_x = 1$ cm, $\delta_y = 2$ cm, $M_y = 10$, and different numbers of sensors M_x. Figure 6.5 shows plots of the DFs and WNGs of the combined superdirective/DS beamformer as a function of frequency for $\delta_x = 1$ cm, $\delta_y = 2$ cm, $M_y = 10$, and different numbers of

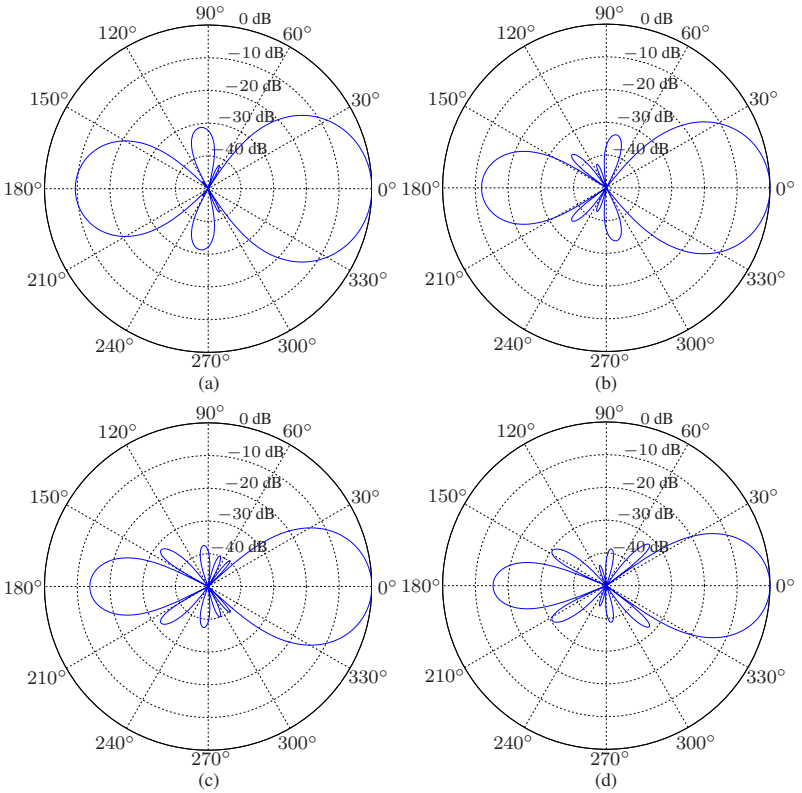

Fig. 6.4 Beampatterns of the combined superdirective/DS beamformer, $\mathbf{h}_{y,\mathrm{DS}} \otimes \mathbf{h}_{x,\mathrm{SD}}$, for $f = 2$ kHz, $\delta_x = 1$ cm, $\delta_y = 2$ cm, $M_y = 10$, and different numbers of sensors M_x: (a) $M_x = 3$, (b) $M_x = 4$, (c) $M_x = 5$, and (d) $M_x = 6$.

sensors M_x. We observe that as the number of sensors increases, the width of the main beam and the level of side lobes decrease, the DF increases, but the WNG decreases. Compared to the DS beamformer, the combined superdirective/DS beamformer yields higher DF, but lower WNG (compare Figs 6.3 and 6.5).

6.4.3 Maximum DF

In the conventional method, the DF is defined as

$$\mathcal{D}(\mathbf{h}) = \frac{\left|\mathbf{h}^H \widetilde{\mathbf{d}}_0\right|^2}{\mathbf{h}^H \widetilde{\mathbf{\Gamma}} \mathbf{h}}. \tag{6.40}$$

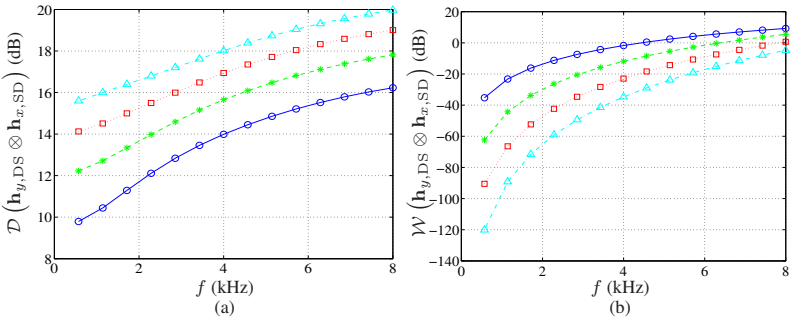

Fig. 6.5 Performance of the combined superdirective/DS beamformer, $\mathbf{h}_{y,\mathrm{DS}} \otimes \mathbf{h}_{x,\mathrm{SD}}$, as a function of frequency for $\delta_x = 1$ cm, $\delta_y = 2$ cm, $M_y = 10$, and different numbers of sensors M_x: $M_x = 3$ (solid line with circles), $M_x = 4$ (dashed line with asterisks), $M_x = 5$ (dotted line with squares), and $M_x = 6$ (dash-dot line with triangles). (a) DF and (b) WNG.

We can easily maximize the previous expression to obtain the maximum DF (mDF) beamformer:

$$\mathbf{h}_{\mathrm{mDF}} = \frac{\widetilde{\mathbf{\Gamma}}^{-1}\widetilde{\mathbf{d}}_0}{\widetilde{\mathbf{d}}_0^H\widetilde{\mathbf{\Gamma}}^{-1}\widetilde{\mathbf{d}}_0}. \tag{6.41}$$

While this approach maximizes the DF, which is equal to $\mathcal{D}\left(\mathbf{h}_{\mathrm{mDF}}\right) = \widetilde{\mathbf{d}}_0^H\widetilde{\mathbf{\Gamma}}^{-1}\widetilde{\mathbf{d}}_0$, it may have a disastrous effect on the WNG. Therefore, $\mathbf{h}_{\mathrm{mDF}}$ may be unpractical.

With the Kronecker product technique, it does not seem obvious to maximize the DF [see eq. (6.20)] but we can maximize the DFs in the directions of the two axes x and y. The maximization of the DF of $\mathbf{h}_x$ gives the superdirective beamformer, $\mathbf{h}_{x,\mathrm{SD}}$, shown in (6.36), while the maximization of the DF of $\mathbf{h}_y$ leads to the mDF beamformer:

$$\mathbf{h}_{y,\mathrm{mDF}} = \frac{\mathbf{\Gamma}_{1,y}^{-1}\mathbf{d}_{y,0}}{\mathbf{d}_{y,0}^H\mathbf{\Gamma}_{1,y}^{-1}\mathbf{d}_{y,0}}, \tag{6.42}$$

where the elements of the $M_y \times M_y$ symmetric Toeplitz matrix $\mathbf{\Gamma}_{1,y}$ are given by

$$\left(\mathbf{\Gamma}_{1,y}\right)_{ij} = \mathrm{sinc}\left(\frac{\omega|i-j|\delta_y}{c}\right), \tag{6.43}$$

with $i, j = 1, 2, \ldots, M_y$. Therefore, the global beamformer is $\mathbf{h}_{y,\mathrm{mDF}} \otimes \mathbf{h}_{x,\mathrm{SD}}$, which, obviously, does not maximize (6.20).

We can improve the previous result, as far the DF is concerned, with a simple iterative algorithm thanks to (6.28) and (6.29). At iteration 0, we take

$$\mathbf{h}_x^{(0)} = \mathbf{h}_{x,\mathrm{SD}}, \tag{6.44}$$

where $\mathbf{h}_{x,\mathrm{SD}}$ is given in (6.36). Substituting $\mathbf{h}_x^{(0)}$ into (6.27), we obtain

$$\mathbf{\Gamma}_x^{(0)} = \left(\mathbf{I}_{M_y} \otimes \mathbf{h}_x^{(0)}\right)^H \widetilde{\mathbf{\Gamma}} \left(\mathbf{I}_{M_y} \otimes \mathbf{h}_x^{(0)}\right). \tag{6.45}$$

Now, substituting this expression into the DF in (6.29), we obtain at iteration 1:

$$\mathcal{D}\left(\mathbf{h}_y^{(1)} | \mathbf{h}_x^{(0)}\right) = \frac{\left|\left(\mathbf{h}_y^{(1)}\right)^H \mathbf{d}_{y,0}\right|^2}{\left(\mathbf{h}_y^{(1)}\right)^H \mathbf{\Gamma}_x^{(0)} \mathbf{h}_y^{(1)}}. \tag{6.46}$$

The maximization of $\mathcal{D}\left(\mathbf{h}_y^{(1)} | \mathbf{h}_x^{(0)}\right)$ with respect to $\mathbf{h}_y^{(1)}$ gives

$$\mathbf{h}_y^{(1)} = \frac{\left(\mathbf{\Gamma}_x^{(0)}\right)^{-1} \mathbf{d}_{y,0}}{\mathbf{d}_{y,0}^H \left(\mathbf{\Gamma}_x^{(0)}\right)^{-1} \mathbf{d}_{y,0}}. \tag{6.47}$$

Using $\mathbf{h}_y^{(1)}$ in (6.26), we get

$$\mathbf{\Gamma}_y^{(1)} = \left(\mathbf{h}_y^{(1)} \otimes \mathbf{I}_{M_x}\right)^H \widetilde{\mathbf{\Gamma}} \left(\mathbf{h}_y^{(1)} \otimes \mathbf{I}_{M_x}\right). \tag{6.48}$$

As a result, the DF in (6.28) is

$$\mathcal{D}\left(\mathbf{h}_x^{(1)} | \mathbf{h}_y^{(1)}\right) = \frac{\left|\left(\mathbf{h}_x^{(1)}\right)^H \mathbf{d}_{x,0}\right|^2}{\left(\mathbf{h}_x^{(1)}\right)^H \mathbf{\Gamma}_y^{(1)} \mathbf{h}_x^{(1)}}, \tag{6.49}$$

whose maximization with respect to $\mathbf{h}_x^{(1)}$ gives

$$\mathbf{h}_x^{(1)} = \frac{\left(\mathbf{\Gamma}_y^{(1)}\right)^{-1} \mathbf{d}_{x,0}}{\mathbf{d}_{x,0}^H \left(\mathbf{\Gamma}_y^{(1)}\right)^{-1} \mathbf{d}_{x,0}}. \tag{6.50}$$

Continuing the iterations up to the iteration n, we easily get for the second filter:

$$\mathbf{h}_y^{(n)} = \frac{\left(\mathbf{\Gamma}_x^{(n-1)}\right)^{-1} \mathbf{d}_{y,0}}{\mathbf{d}_{y,0}^H \left(\mathbf{\Gamma}_x^{(n-1)}\right)^{-1} \mathbf{d}_{y,0}}, \tag{6.51}$$

with

$$\mathbf{\Gamma}_x^{(n-1)} = \left(\mathbf{I}_{M_y} \otimes \mathbf{h}_x^{(n-1)}\right)^H \widetilde{\mathbf{\Gamma}} \left(\mathbf{I}_{M_y} \otimes \mathbf{h}_x^{(n-1)}\right), \tag{6.52}$$

and for the first filter:

$$\mathbf{h}_x^{(n)} = \frac{\left(\mathbf{\Gamma}_y^{(n)}\right)^{-1} \mathbf{d}_{x,0}}{\mathbf{d}_{x,0}^H \left(\mathbf{\Gamma}_y^{(n)}\right)^{-1} \mathbf{d}_{x,0}}, \tag{6.53}$$

with

$$\mathbf{\Gamma}_y^{(n)} = \left(\mathbf{h}_y^{(n)} \otimes \mathbf{I}_{M_x}\right)^H \widetilde{\mathbf{\Gamma}} \left(\mathbf{h}_y^{(n)} \otimes \mathbf{I}_{M_x}\right). \tag{6.54}$$

As a result, the global beamformer at iteration n is $\mathbf{h}_y^{(n)} \otimes \mathbf{h}_x^{(n)}$. Since the DFs of the individual beamformers increase at each iteration, so is the DF of the global beamformer and we should expect (6.20) to be maximized for n large enough. While this iterative algorithm may lead to a high value of the DF, white noise amplification may be a serious issue.

Figure 6.6 displays the directivity patterns of the global mDF beamformer at the iteration $n = 5$, $\mathbf{h}_y^{(5)} \otimes \mathbf{h}_x^{(5)}$, for $f = 2$ kHz, $\delta_x = \delta_y = 1$ cm, $M_y = 3$, and different numbers of sensors M_x. Figure 6.7 shows plots of the DFs and WNGs of the global mDF beamformer for $\delta_x = \delta_y = 1$ cm, $M_y = 3$, and different numbers of sensors M_x. We observe that as the number of sensors increases, the DF of the global mDF beamformer increases, but the WNG decreases. Compared to the DS beamformer and the combined superdirective/DS beamformer, the global mDF beamformer yields higher DF, but lower WNG (compare Figs 6.3, 6.5, and 6.7).

One obvious way to better compromise between the DF and the WNG is to change the initialization to

$$\mathbf{h}_x^{(0)} = \mathbf{h}_{x,\mathrm{DS}}, \tag{6.55}$$

where $\mathbf{h}_{x,\mathrm{DS}}$ is the individual DS beamformer defined in (6.33). We can iterate as above using (6.28) and (6.29) and stop when we achieve a desired DF or when we do not desire to go below a certain level of the WNG.

6.4.4 Null Steering

In this subsection, we assume that we have one interference source impinging on the array from the direction $\theta_0 \neq 0$ that we would like to completely cancel, i.e., to steer a null in that direction, and, meanwhile, recover the desired source coming from the endfire direction. With the conventional approach,

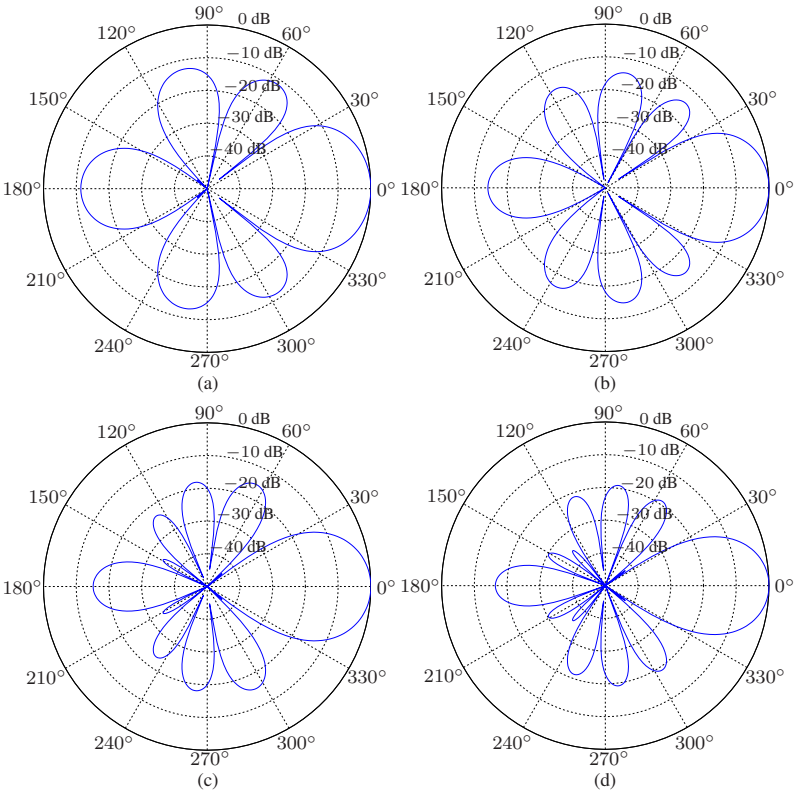

Fig. 6.6 Beampatterns of the global mDF beamformer at the iteration $n = 5$, $\mathbf{h}_y^{(5)} \otimes \mathbf{h}_x^{(5)}$, for $f = 2$ kHz, $\delta_x = \delta_y = 1$ cm, $M_y = 3$, and different numbers of sensors M_x: (a) $M_x = 3$, (b) $M_x = 4$, (c) $M_x = 5$, and (d) $M_x = 6$.

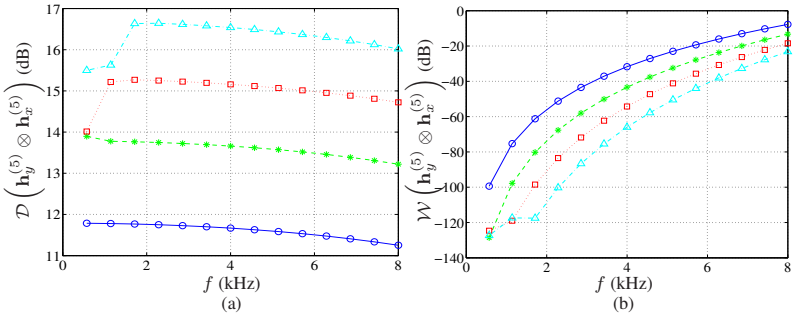

Fig. 6.7 Performance of the global mDF beamformer at the iteration $n = 5$, $\mathbf{h}_y^{(5)} \otimes \mathbf{h}_x^{(5)}$, as a function of frequency for $\delta_x = \delta_y = 1$ cm, $M_y = 3$, and different numbers of sensors M_x: $M_x = 3$ (solid line with circles), $M_x = 4$ (dashed line with asterisks), $M_x = 5$ (dotted line with squares), and $M_x = 6$ (dash-dot line with triangles). (a) DF and (b) WNG.

the constraint equation for a distortionless response and a null at θ_0 is

$$\widetilde{\mathbf{C}}^H \mathbf{h} = \mathbf{i}_{\mathrm{c}}, \tag{6.56}$$

where

$$\widetilde{\mathbf{C}} = \left[\widetilde{\mathbf{d}}_0 \; \widetilde{\mathbf{d}}_{\theta_0} \right] \tag{6.57}$$

is the constraint matrix of size $M_x M_y \times 2$ whose two columns are linearly independent and

$$\mathbf{i}_{\mathrm{c}} = \left[1 \; 0 \right]^T \tag{6.58}$$

is a vector of length 2. There are two interesting ways to find $\mathbf{h}$. The first obvious beamformer is obtained by maximizing the WNG and by taking (6.56) into account, i.e.,

$$\min_{\mathbf{h}} \mathbf{h}^H \mathbf{h} \quad \text{subject to} \quad \widetilde{\mathbf{C}}^H \mathbf{h} = \mathbf{i}_{\mathrm{c}}. \tag{6.59}$$

From this criterion, we find the minimum-norm (MN) beamformer:

$$\mathbf{h}_{\mathrm{MN}} = \widetilde{\mathbf{C}} \left(\widetilde{\mathbf{C}}^H \widetilde{\mathbf{C}} \right)^{-1} \mathbf{i}_{\mathrm{c}}, \tag{6.60}$$

which is also the minimum-norm solution of (6.56). The other beamformer is obtained by maximizing the DF and by taking (6.56) into account, i.e.,

$$\min_{\mathbf{h}} \mathbf{h}^H \widetilde{\mathbf{\Gamma}} \mathbf{h} \quad \text{subject to} \quad \widetilde{\mathbf{C}}^H \mathbf{h} = \mathbf{i}_{\mathrm{c}}. \tag{6.61}$$

We easily find the null-steering (NS) beamformer:

$$\mathbf{h}_{\mathrm{NS}} = \widetilde{\mathbf{\Gamma}}^{-1} \widetilde{\mathbf{C}} \left(\widetilde{\mathbf{C}}^H \widetilde{\mathbf{\Gamma}}^{-1} \widetilde{\mathbf{C}} \right)^{-1} \mathbf{i}_{\mathrm{c}}. \tag{6.62}$$

Obviously, we always have

$$\mathcal{W}\left(\mathbf{h}_{\mathrm{NS}}\right) \leq \mathcal{W}\left(\mathbf{h}_{\mathrm{MN}}\right), \tag{6.63}$$

$$\mathcal{D}\left(\mathbf{h}_{\mathrm{NS}}\right) \geq \mathcal{D}\left(\mathbf{h}_{\mathrm{MN}}\right). \tag{6.64}$$

For the Kronecker product approach, there are many possibilities. Now, for our above formulated problem, the corresponding constraint equations on the two filters $\mathbf{h}_x$ and $\mathbf{h}_y$ are

$$\mathbf{C}_x^H \mathbf{h}_x = \mathbf{i}_{\mathrm{c}}, \tag{6.65}$$

$$\mathbf{C}_y^H \mathbf{h}_y = \mathbf{i}_{\mathrm{c}}, \tag{6.66}$$

where

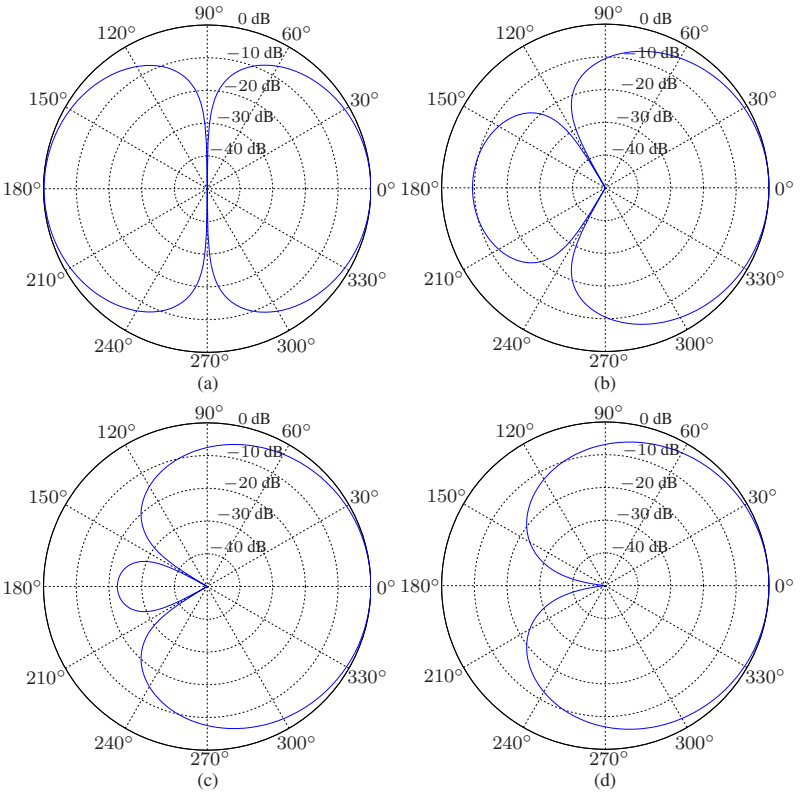

Fig. 6.8 Beampatterns of the global MN beamformer, $\mathbf{h}_{y,\mathrm{DS}} \otimes \mathbf{h}_{x,\mathrm{MN}}$, for $f = 2$ kHz, $\delta_x = \delta_y = 1$ cm, $M_x = 3$, $M_y = 5$, and several values of θ_0: (a) $\theta_0 = 90°$, (b) $\theta_0 = 120°$, (c) $\theta_0 = 150°$, and (d) $\theta_0 = 180°$.

$$\mathbf{C}_x = \left[\, \mathbf{d}_{x,0} \; \mathbf{d}_{x,\theta_0} \,\right], \tag{6.67}$$

$$\mathbf{C}_y = \left[\, \mathbf{d}_{y,0} \; \mathbf{d}_{y,\theta_0} \,\right] \tag{6.68}$$

are the constraint matrices of size $M_x \times 2$ and $M_y \times 2$, respectively. From (6.65) and (6.66), we easily find the individual MN beamformers:

$$\mathbf{h}_{x,\mathrm{MN}} = \mathbf{C}_x \left(\mathbf{C}_x^H \mathbf{C}_x\right)^{-1} \mathbf{i}_{\mathrm{c}}, \tag{6.69}$$

$$\mathbf{h}_{y,\mathrm{MN}} = \mathbf{C}_y \left(\mathbf{C}_y^H \mathbf{C}_y\right)^{-1} \mathbf{i}_{\mathrm{c}}. \tag{6.70}$$

As a consequence, for the global MN beamformer, we have three interesting possibilities: $\mathbf{h}_{y,\mathrm{DS}} \otimes \mathbf{h}_{x,\mathrm{MN}}$, $\mathbf{h}_{y,\mathrm{MN}} \otimes \mathbf{h}_{x,\mathrm{DS}}$, and $\mathbf{h}_{y,\mathrm{MN}} \otimes \mathbf{h}_{x,\mathrm{MN}}$. The three of them, obviously, put a null in the direction θ_0, but for the last one, the null is of multiplicity 2, and its corresponding WNG (resp. DF) should be smaller (resp. greater) than the two others.

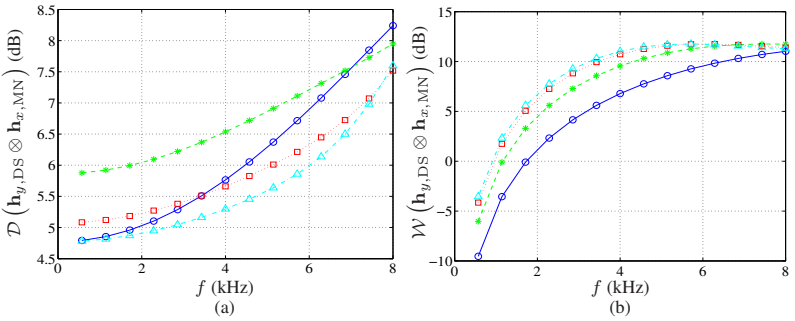

Fig. 6.9 Performance of the global MN beamformer, $\mathbf{h}_{y,\mathrm{DS}} \otimes \mathbf{h}_{x,\mathrm{MN}}$, as a function of frequency for $\delta_x = \delta_y = 1$ cm, $M_x = 3$, $M_y = 5$, and several values of θ_0: $\theta_0 = 90°$ (solid line with circles), $\theta_0 = 120°$ (dashed line with asterisks), $\theta_0 = 150°$ (dotted line with squares), and $\theta_0 = 180°$ (dash-dot line with triangles). (a) DF and (b) WNG.

Figure 6.8 displays the directivity patterns of the global MN beamformer, $\mathbf{h}_{y,\mathrm{DS}} \otimes \mathbf{h}_{x,\mathrm{MN}}$, for $f = 2$ kHz, $\delta_x = \delta_y = 1$ cm, $M_x = 3$, $M_y = 5$, and several values of θ_0. Figure 6.9 shows plots of the DFs and WNGs of the global MN beamformer as a function of frequency for $\delta_x = \delta_y = 1$ cm, $M_x = 3$, $M_y = 5$, and several values of θ_0. We observe a null in the direction θ_0, and the WNG of the global MN beamformer increases as θ_0 increases from 90° to 180°.

Following the steps of the conventional approach, we easily find the individual NS beamformers:

$$\mathbf{h}_{x,\mathrm{NS}} = \mathbf{\Gamma}_1^{-1}\mathbf{C}_x\left(\mathbf{C}_x^H\mathbf{\Gamma}_1^{-1}\mathbf{C}_x\right)^{-1}\mathbf{i}_{\mathrm{c}}, \tag{6.71}$$

$$\mathbf{h}_{y,\mathrm{NS}} = \mathbf{\Gamma}_{1,y}^{-1}\mathbf{C}_y\left(\mathbf{C}_y^H\mathbf{\Gamma}_{1,y}^{-1}\mathbf{C}_y\right)^{-1}\mathbf{i}_{\mathrm{c}}, \tag{6.72}$$

and for the global beamformer, we have many more possibilities depending on what we want. Here are some examples: $\mathbf{h}_{y,\mathrm{NS}} \otimes \mathbf{h}_{x,\mathrm{SD}}$, $\mathbf{h}_{y,\mathrm{NS}} \otimes \mathbf{h}_{x,\mathrm{MN}}$, $\mathbf{h}_{y,\mathrm{mDF}} \otimes \mathbf{h}_{x,\mathrm{NS}}$, $\mathbf{h}_{y,\mathrm{MN}} \otimes \mathbf{h}_{x,\mathrm{NS}}$, $\mathbf{h}_{y,\mathrm{DS}} \otimes \mathbf{h}_{x,\mathrm{NS}}$, and $\mathbf{h}_{y,\mathrm{NS}} \otimes \mathbf{h}_{x,\mathrm{NS}}$. The last one will give the best DF.

Figure 6.10 displays the global NS beamformer, $\mathbf{h}_{y,\mathrm{DS}} \otimes \mathbf{h}_{x,\mathrm{NS}}$, for $f = 2$ kHz, $\delta_x = \delta_y = 1$ cm, $M_x = 3$, $M_y = 5$, and several values of θ_0. Figure 6.11 shows plots of the DFs and WNGs of the global NS beamformer, $\mathbf{h}_{y,\mathrm{DS}} \otimes \mathbf{h}_{x,\mathrm{NS}}$, as a function of frequency for $\delta_x = \delta_y = 1$ cm, $M_x = 3$, $M_y = 5$, and several values of θ_0. Figure 6.12 displays the global NS beamformer, $\mathbf{h}_{y,\mathrm{NS}} \otimes \mathbf{h}_{x,\mathrm{NS}}$, for $f = 2$ kHz, $\delta_x = \delta_y = 1$ cm, $M_x = 3$, $M_y = 5$, and several values of θ_0. Figure 6.13 shows plots of the DFs and WNGs of the global NS beamformer, $\mathbf{h}_{y,\mathrm{NS}} \otimes \mathbf{h}_{x,\mathrm{NS}}$, as a function of frequency for $\delta_x = \delta_y = 1$ cm, $M_x = 3$, $M_y = 5$, and several values of θ_0. We observe a null in the direction θ_0. Compared to the global MN beamformers, the global NS beamformers yield higher DF, but lower WNG. The beamformer $\mathbf{h}_{y,\mathrm{NS}} \otimes \mathbf{h}_{x,\mathrm{NS}}$ yields the highest DF, but lowest WNG (compare Figs 6.9, 6.11, and 6.13).

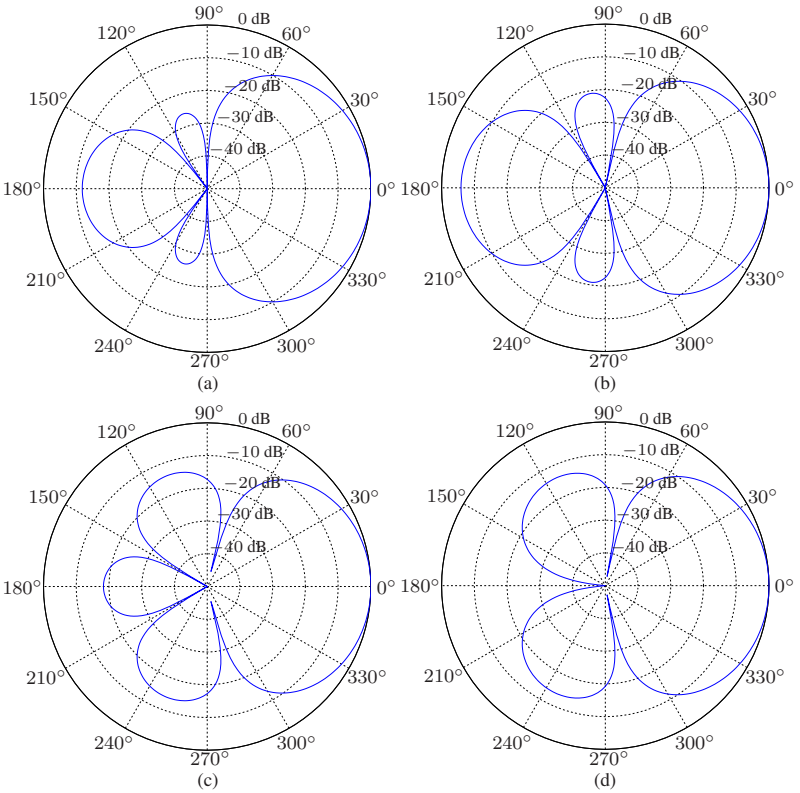

Fig. 6.10 Beampatterns of the global NS beamformer, $\mathbf{h}_{y,\mathrm{DS}} \otimes \mathbf{h}_{x,\mathrm{NS}}$, for $f = 2$ kHz, $\delta_x = \delta_y = 1$ cm, $M_x = 3$, $M_y = 5$, and several values of θ_0: (a) $\theta_0 = 90°$, (b) $\theta_0 = 120°$, (c) $\theta_0 = 150°$, and (d) $\theta_0 = 180°$.

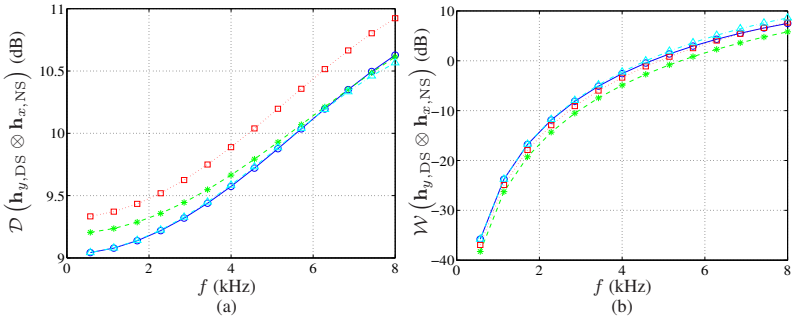

Fig. 6.11 Performance of the global NS beamformer, $\mathbf{h}_{y,\mathrm{DS}} \otimes \mathbf{h}_{x,\mathrm{NS}}$, as a function of frequency for $\delta_x = \delta_y = 1$ cm, $M_x = 3$, $M_y = 5$, and several values of θ_0: $\theta_0 = 90°$ (solid line with circles), $\theta_0 = 120°$ (dashed line with asterisks), $\theta_0 = 150°$ (dotted line with squares), and $\theta_0 = 180°$ (dash-dot line with triangles). (a) DF and (b) WNG.

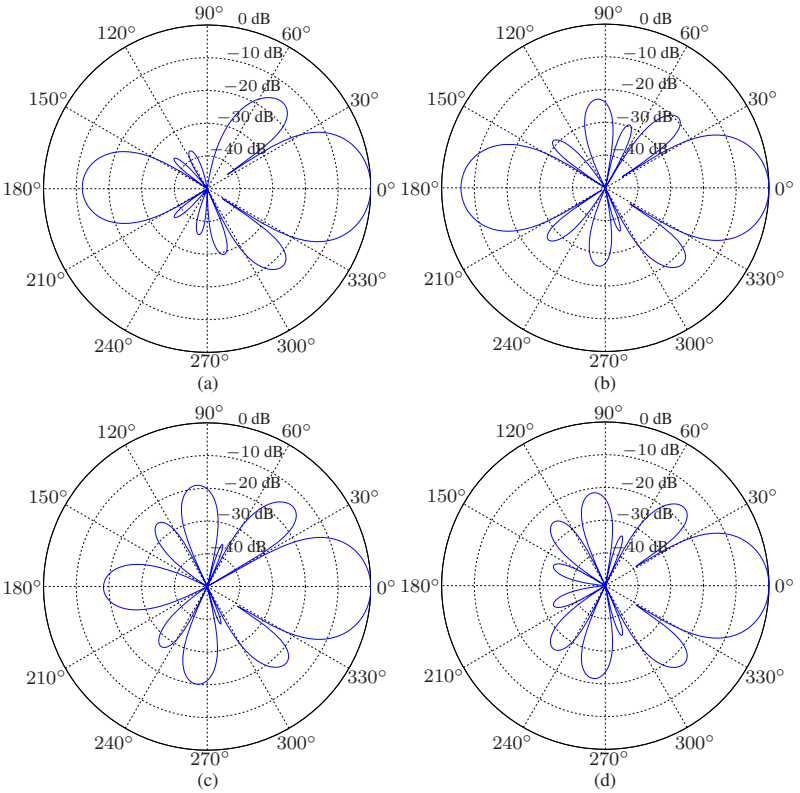

Fig. 6.12 Beampatterns of the global NS beamformer, $\mathbf{h}_{y,\mathrm{NS}} \otimes \mathbf{h}_{x,\mathrm{NS}}$, for $f = 2$ kHz, $\delta_x = \delta_y = 1$ cm, $M_x = 3$, $M_y = 5$, and several values of θ_0: (a) $\theta_0 = 90°$, (b) $\theta_0 = 120°$, (c) $\theta_0 = 150°$, and (d) $\theta_0 = 180°$.

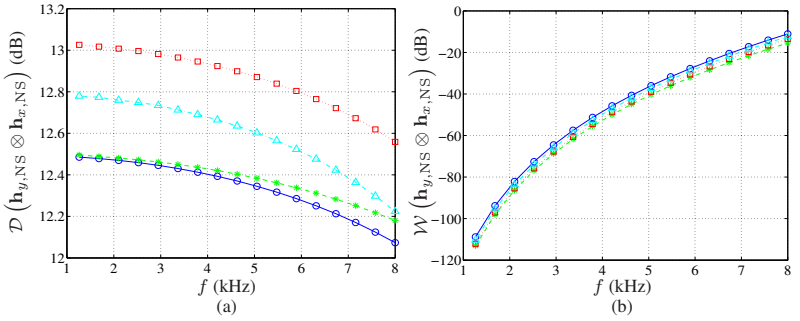

Fig. 6.13 Performance of the global NS beamformer, $\mathbf{h}_{y,\mathrm{NS}} \otimes \mathbf{h}_{x,\mathrm{NS}}$, as a function of frequency for $\delta_x = \delta_y = 1$ cm, $M_x = 3$, $M_y = 5$, and several values of θ_0: $\theta_0 = 90°$ (solid line with circles), $\theta_0 = 120°$ (dashed line with asterisks), $\theta_0 = 150°$ (dotted line with squares), and $\theta_0 = 180°$ (dash-dot line with triangles). (a) DF and (b) WNG.

References

1. H. L. Van Trees, *Optimum Array Processing: Part IV of Detection, Estimation, and Modulation Theory*. New York, NY: John Wiley & Sons, Inc., 2002.
2. J. Benesty, I. Cohen, and J. Chen, *Fundamentals of Signal Enhancement and Array Signal Processing*. Singapore: Wiley-IEEE Press, 2018.
3. H. Cox, R. M. Zeskind, and T. Kooij, "Practical supergain," *IEEE Trans. Acoust., Speech, Signal Process.*, vol. ASSP-34, pp. 393–398, June 1986.
4. H. Cox, R. M. Zeskind, and M. M. Owen, "Robust adaptive beamforming," *IEEE Trans. Acoust., Speech, Signal Process.*, vol. ASSP-35, pp. 1365–1376, Oct. 1987.
5. J. Benesty, J. Chen, and C. Pan, *Fundamentals of Differential Beamforming*. Springer Briefs in Electrical & Computer Engineering, 2016.